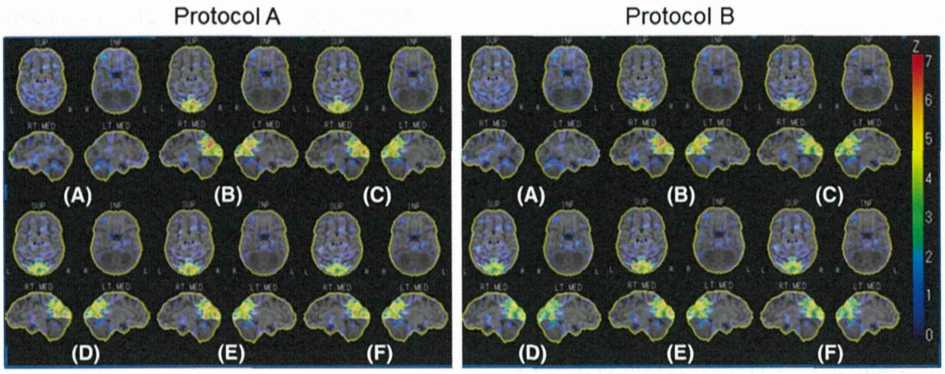

Fig. 3 *Z* score map of changes in inferior, superior and, left- and right-med sagittal images in PD in protocols A and B. Pixel values are normalized to global brain, and images show decreases in *Z* scores. *Z* score images confirm hypoperfused regions. The *Z* score in each *Z* score map image is scaled from 0.0 to 7.0. Protocol A: No hypoperfusion [PD (High)–NDB (High)] (**a**); PD (High)–NDB (High) [PD (30 m)–NBD (30 m)] (**b**); PD (Medium)–NDB (Medium) (**c**); PD (Low)–NDB (Low) (**d**); PD (20 m)–NDB (20 m) (**e**); PD (15 m)–NDB (15 m) (**f**). Protocol B, No hypoperfusion (PD (High)–NDB (High)) (**a**); PD (High)–NDB (High) [PD (30 m)–NBD (30 m)] (**b**); PD (Medium)–NDB (High) (**c**); PD (Low)–NDB (High) (**d**); PD (20 m)–NBD (30 m) (**e**); PD (15 m)–NBD (30 m) (**f**)

to 0.08, 0.09, and 0.10 in response to decreases in the injected dose and acquisition time.

3.3 *Z* scores and detection error

Figure 3 shows *Z* score maps of hypoperfusion regions on images generated from protocols A and B. The *Z* scores tended to decrease when conditions (injected dose and acquisition time) were decreased in protocols A and B. A decreased injection dose and acquisition time in protocol A resulted in a gradual reduction in *Z* scores. The average *Z* scores of PD (Low)–NDB (Low) vs. PD (High)–NDB (High) ($p = 0.015$), PD (20 m)–NDB (20 m) vs. PD (30 m)–NDB (30 m) ($p = 0.021$) and PD (15 m)–NDB (15 m) vs. PD (30 m)–NDB (30 m) ($p = 0.009$) were decreased significantly in protocol A. The average *Z* scores did not differ significantly between PD (Medium)–NDB (Medium) vs. PD (High)–NDB (High) and PD (Medium)–NDB (Medium) vs. PD (Low)–NDB (Low) in Fig. 4a. The average Z scores of PD (Medium)–NDB (High) vs. PD (High)–NDB (High) did not differ significantly ($p = 0.061$), but those of PD (Low)–NDB (High) vs. PD (High)–NDB (High), PD (Medium)–NDB (High) vs. PD (Low)–NDB (High), PD (15 m)–NDB (30 m) vs. PD (30 m)–NDB (30 m), PD (20 m)–NDB (30 m) vs. PD (30 m)–NDB (30 m), and PD (15 m)–NDB (30 m) vs. PD (20 m)–NDB (30 m) ($p = 0.001$, $p = 0.008$, $p = 0.005$, $p = 0.041$, and $p = 0.038$, respectively) decreased significantly in protocol B (Fig. 4b).

Table 2 shows changes in error between measured and selected hypoperfused areas in response to different conditions in protocols A and B. The detection error resulted in underestimations under all conditions except for PD (High)–NDB (High) [PD (30 m)–NDB (30 m)]. The detection error was larger in protocol B than in protocol A and increased from 6.65 % [PD (Medium)–NDB (Medium)] in protocol A to 32.05 % (PD (15 m)–NDB (30 m)) in protocol B. When the injected doses and acquisition times were the same as those of the NDB, the maximal detection error was 17 %. However, this increased to 32 % when the conditions differed from those of the NDB. These findings confirmed that the detection error was reduced when the injected dose (acquisition time) and the NDB were the same.

4 Discussion

Radiopharmaceutical doses are uniform in Japan because of health insurance coverage. However, injected doses vary among institutions, and metropolitan as well as regional insurance might not cover increases or decreases in injected doses. We simulated different injected doses from continuous SPECT datasets and evaluated the impact of these doses and various acquisition times using *Z* scores and detection errors.

The linearity between the dose and the SPECT count (Fig. 1b) was excellent. This finding justified the determination of variations among injected doses and acquisition times from projection datasets in each simulated SPECT image and NDB.

In general, SPECT images become degraded by a decrease in the signal to noise ratio to increase the high-frequency component caused by a low injected dose and short acquisition time. The injected dose and acquisition time significantly affected the SD of the NDB. When the injected dose and acquisition time were decreased, the images used for the NDB probably included high-

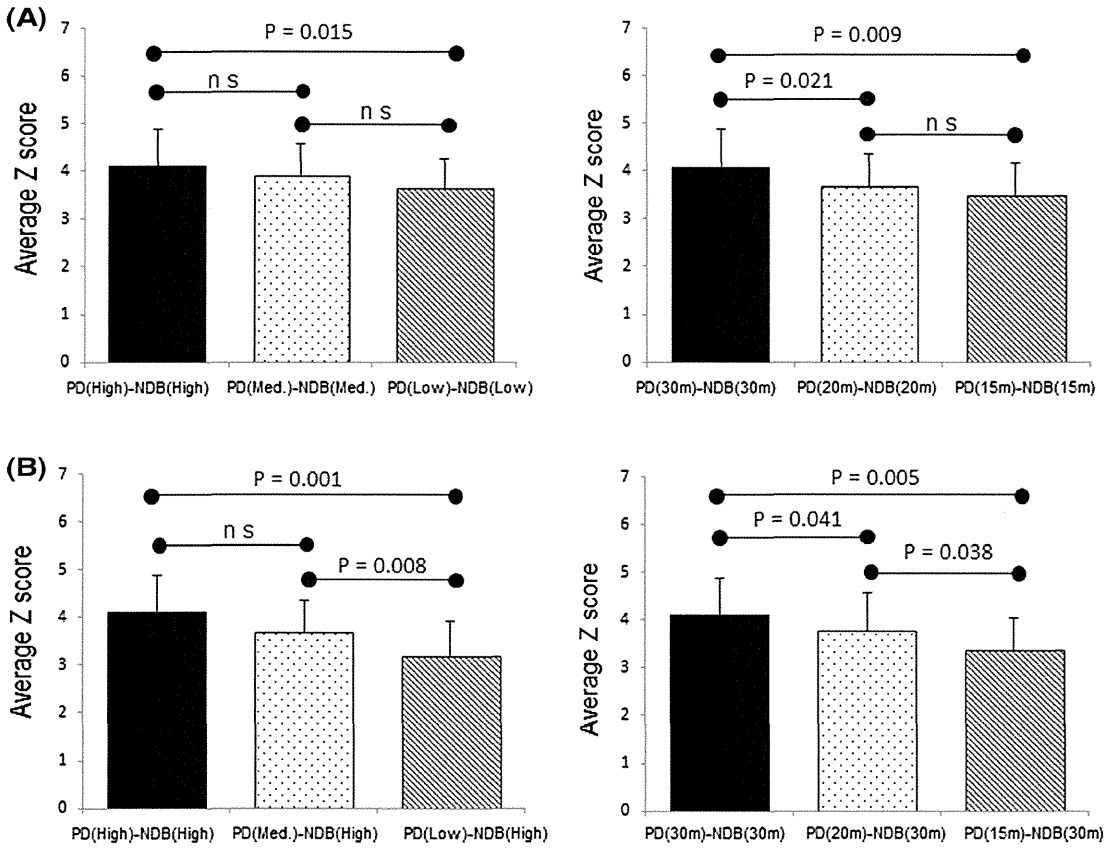

Fig. 4 Differences in Z scores of hypoperfused areas among protocols A, B, and PD (High)–NDB (High). Data are shown as mean ± SD ($n = 7$); $p < 0.05$

Table 2 Detection errors compared with true values in hypoperfused area

Protocol A					
PD (High)–NDB (High)	PD (Medium)–NDB (Medium)	PD (Low)–NDB (Low)	PD (30 m)–NDB (30 m)	PD (20 m)–NDB (20 m)	PD (15 m)–NDB (15 m)
0.00	−6.65	−13.57	0.00	−7.36	−16.45
Protocol B					
PD (High)–NDB (High)	PD (Medium)–NDB (High)	PD (Low)–NDB (High)	PD (30 m)–NDB (30 m)	PD (20 m)–NDB (30 m)	PD (15 m)–NDB (30 m)
0.00	−8.61	−32.05	0.00	-8.37	−24.31

Units are % error of measurement compared with true region size

frequency components that caused the mode of the SD distribution of the NDB to shift to higher values. The SD distribution was naturally Gaussian. However, the shape of the SD distribution was spread asymmetrically in this study. We considered that the dispersion of data was reduced so that patient's data were acquired at each of the participating institutions, as reported by Onishi et al. [9]. The Z scores of statistical cerebral function analysis depended on the SD distribution that was maintained by the NDB in our study groups [10, 12].

The average Z scores decreased slightly when the conditions matched those of the PD and NDB (protocol A). The average Z score was lower for PD (Medium) than for PD (High) in protocol A, but the difference did not reach significance. However, the calculated Z scores were affected by matching the injected dose and acquisition time between the PD and the NDB. The average Z score became considerably decreased when the PD and NDB were mismatched in protocol B. When the injected dose was the same as that in the NDB, the smaller average Z score was

probably generated because the SD was higher for a lower (short acquisition time) than for a larger (long acquisition time) injected dose. Because *Z* scores and detection errors determined during the assembly of PD (Medium)–NDB (Medium) and PD (Medium)–NDB (High) were >10 %, we considered that the performance was equal to that of the PD (High)–NDB (High).

These results suggest that *Z* scores and detection errors are affected when the injected dose (acquisition time) is the same as that of the NDB. The acquisition time has to effect on *Z* score and detectability than the injected dose without NDB (15 m) as shown in Fig. 4 and Table 2. If we assumed that injected dose was equal to an input signal, we considered that detectability was approximately proportional to intensity of input signal. The distribution of I-123-IMP in brain tissue reflects regional cerebral blood flow very well, and its distributional pattern changes as time goes on. This factor should be considered in the assessment of I-123-IMP distribution. The first six rotations were set as early phase and the last six rotations were set as later phase. Even though SPECT data acquisition started 15 min after and continued for about 30 min, the difference in counts between the early and later phases of dynamic SPECT data sets was significant in this simulation study. We suggested that the acquisition time has more effect on the *Z* score than the injected dose, in particular for NDB (15 m). However, when health insurance has limited the injected dose, accurate *Z* scores can be achieved by use of a combination of NDB (High) and an injected dose of 167, 222 MBq in clinical studies.

Notwithstanding the findings of the study, certain limitations need to be acknowledged. SPECT datasets for various injected doses and acquisition times were simulated and might differ from those in actual clinical studies. In this study, projection data sets were merged at each rotation data set for the simulated injected dose and acquisition time. We did not consider on the scatter at the early and late phases. Scatter content was different at the projection data sets of the rotation in the I-123-IMP clinical SPECT study. Scatter was overestimated in simulated projection data sets from patients injected with doses other than 222 MBq. We performed a strict scatter correction at each rotation in the dynamic SPECT. In simulated acquisition time at NDB, this result was different with merged at any rotations for NDB data sets, too. Another limitation is that we did not apply with CT-based attenuation correction (CTAC). Ishii et al. [14] and Shimosegawa et al. [15] reported that a CTAC is needed for accurate brain perfusion images. However, we believe that the present findings are similar to those of Ishii et al.

5 Conclusions

Z scores were specific for the injected dose and acquisition time in a 3D-SSP study, and the calculated *Z* scores were affected by matching the injected dose and acquisition time between the PD and the NDB. However, we suggest that accurate *Z* scores can be obtained in clinical studies by use of the NDB (High) with an injected dose of 167 MBq.

Acknowledgments The authors wish to thank Dr. Uji Asano of Kitasato University and Dr. Kazunari Ishii of Kinki University and Dr. Masanobu Syabana of Matsue City Hospital.

Conflict of interest The authors declare that they have no conflict of interest.

References

1. Minoshima S, Giordani B, Berent S, Frey KA, Foster NL, Kuhl DE. Metabolic reduction in the posterior cingulate cortex in very early Alzheimer's disease. Ann Neurol. 1997;42:85–94.
2. Matsuda H. Cerebral blood flow and metabolic abnormalities in Alzheimer's disease. Ann Nucl Med. 2001;15:85–92.
3. Ishii K. Clinical application of positron emission tomography for diagnosis of dementia. Ann Nucl Med. 2002;16:515–25.
4. Kogure D, Matsuda H, Ohnishi T, Asada T, Uno M, Kunihiro T, et al. Longitudinal evaluation of early Alzheimer's disease using brain perfusion SPECT. J Nucl Med. 2000;41:1155–62.
5. Hirao K, Ohnishi T, Matsuda H, Nemoto K, Hirata Y, Yamashita F, et al. Functional interaction between entorhinal cortex and posterior cingulate cortex at the very early stage of Alzheimer's disease using brain perfusion single-photon emission computed tomography. Nucl Med Commun. 2006;27:151–6.
6. Imabayashi E, Matsuda H, Asada T, Ohnishi T, Sakamoto S, Nakano S, et al. Superiority of 3-dimensional stereotactic surface projection analysis over visual inspection in discrimination of patients with very early Alzheimer's disease from controls using brain perfusion SPECT. J Nucl Med. 2004;45:1450–7.
7. Nishimura M, Matsuda H, Imabayashi E, Kuji I, Sato N. Comparison of SPM and NEUROSTAT in voxel wise statistical analysis of brain SPECT and MRI at the early stage of Alzheimer's disease. Ann Nucl Med. 2008;22:921–7.
8. Minoshima S, Frey KA, Koeppe RA, Foster NL, Kuhl DE. A diagnostic approach in Alzheimer's disease using three-dimensional stereotactic surface projections of fluorine-18-FDG PET. J Nucl Med. 1995;36:1238–48.
9. Onishi H, Matsutomo N, Kai Y, Kangai Y, Amijima H, Yamaguchi T. Evaluation of a novel normal database with matched SPECT systems and optimal pre-filter parameters for 3D-SSP. Ann Nucl Med. 2012;26:16–25.
10. Onishi H, Hatazawa J, Nakagawara J, Ito K, Kawa S, Masuda Y, et al. Availability of normal database by single photon emission computed tomography system with use of 3 dimensional-stereotactic surface projections. Nihon Hōshasen Gijutsu Gakkai Zasshi. 2012;68:1608–16 (in Japanese).
11. Mizumura S, Kumita S, Cho K, Ishihara M, Nakajo H, Toba M, et al. Development of quantitative analysis method for stereotactic brain image: assessment of reduced accumulation in extent and severity using anatomical segmentation. Ann Nucl Med. 2003;17:289–95.

12. Onishi H, Matsutake Y, Matsutomo N, Kai Y, Amijima H. Effect of pre-filtering cut-off frequency and scatter and attenuation corrections during normal database creation for statistical imaging analysis of the brain. J Nucl Med Technol. 2011;39:231–6.
13. Shimada H, Okake H, Higuchi T, Arisaka Y, Oriuchi N, Endo K. Normal database (NDB) of 123I-IMP brain perfusion SPECT examination is affected by statistical image analysis in the presence or absence of scatter correction and attenuation correction. Kaku Igaku. 2012;49:341–9 (in Japanese).
14. Ishii K, Hanaoka K, Okada M, Kumano S, Komeya Y, Tsuchiya N, et al. Impact of CT attenuation correction by SPECT/CT in brain perfusion images. Ann Nucl Med. 2012;26:241–7.
15. Shimosegawa E, Fujino K, Kato H, Hatazawa J. Quantitative CBF measurement using an integrated SPECT/CT system: validation of three-dimensional ordered-subset expectation maximization and CT-based attenuation correction by comparing with O-15 water PET. Ann Nucl Med. 2013;27:822–33.

平成26年度　厚生労働科学研究費補助金（長寿科学総合研究事業）
介護予防プログラム開発に関する研究
平成26年度　総括・分担研究報告書

発行責任者　研究代表者　島田　裕之
発　　行　愛知県大府市森岡町7丁目430番地
国立長寿医療研究センター
TEL　0562－46－8294
FAX　0562－46－8294